33RD CONGRESS
OF THE INTERNATIONAL COUNCIL
OF THE AERONAUTICAL SCIENCES
STOCKHOLM, SWEDEN, 4-9 SEPTEMBER, 2022

ICAS 2022 SWEDEN

A STUDY ON THE NUMERICAL SIMULATION OF FLOW TRANSITION INCLUDING CROSSFLOW EFFECTS

Aline R. Santos Righi[1], Gustavo Luiz Olichevis Halila[2] & João Luiz F. Azevedo[3]

[1]Instituto Tecnológico de Aeronáutica, 12228-900, São José dos Campos, SP, Brazil
[2]Embraer S.A., Research & Development, 12227-901, São José dos Campos, SP, Brazil
[3]Instituto de Aeronáutica e Espaço, 12228-904, São José dos Campos, SP, Brazil

Abstract

For many decades now, the aerospace academia and industry have been using CFD tools for analysis and optimization of aerospace configurations. However, there are some areas in which some challenges remain. One of these challenges is the correct treatment of the laminar-turbulent transition over high Reynolds number flow conditions. The laminar-turbulent transition can be triggered by different mechanisms, for example, stationary crossflow vortices. In order to study transitional flows, the Langtry-Menter transition model, coupled with the SST model for turbulence closure, is already implemented in an in-house code, BRU3D. The Langtry-Menter transition model, as previously available in the code, was only able to represent transition caused by the amplification of Tollmien-Schlichting waves and bypass transition. This was possible due additional transport equations fed by empirical correlations. The present work considers the implementation of the extended Langtry-Menter transition model with an empirical correlation for transition due to crossflow vortices. The investigation includes the impact in the solution of different freestream turbulent properties, as well as the numerical convergence, considering the newly added equations.

Keywords: CFD, Laminar-Turbulent Transition, Langtry-Menter Model, Crossflow, Prolate Spheroid

1. Introduction

Computational Fluid Dynamics (CFD) techniques have been used for many different academic and industrial purposes for the past decades. Although such techniques have been continuously improving throughout the years, some significant challenges remain, specially in the aerospace industry [1]. One of such challenging areas is the correct treatment of the laminar-turbulent transition. In the path to turbulence, a laminar boundary layer base flow is excited by external factors, such as roughness, sound, vibration, and freestream turbulence through a mechanism called receptivity. For example, in aerospace applications, the amplification of Tollmien-Schlichting (TS) waves [2], bypass transition [3], crossflow vortices [4] and leading edge transition and flow contamination [5] are the most common transition mechanisms. It is important to correctly represent the transition mechanism, considering that this phenomena play an important role in several engineering applications. For instance, in high-lift devices, the inclusion of transition effects in numerical simulations improves the agreement with experimental data [6]. In yet another example, aircraft configurations not designed to preserve laminar flow may present transitional regions [7, 8], among others.

There are many modeling strategies available and transition prediction can be achieved through the e^n method or empirical correlations. However, some of the available methods do not include all of the necessary effects in transition prediction or represent high computational costs. For instance, the approaches based on the stability equations connected to the e^n method [9, 10] are not compatible with general-purpose CFD methods. Reynolds-averaged Navier-Stokes (RANS) turbulence models are based on a time-averaging procedure and, as a result, only an average frequency is seen by the model; therefore, important spectral information is lost [7].

The transition process should preferably not be viewed as external to the range of the RANS methods. To alleviate this shortcoming, modified RANS models were proposed with the idea of allowing accurate and inexpensive transitional flow predictions. These models usually augment a standard, fully-turbulent RANS model with one or two additional transport equations based on empirical correlations and only on local parameters. With these considerations in mind, the Langtry-Menter transition model [11] (LCTM - Local Correlation-based Transition Model) was developed. The first published model only represents transition caused by the amplification of Tollmien-Schlichting waves and bypass transition. However, many extensions of the Langtry-Menter model have been developed throughout the years and published in the literature. One of these extensions accounts for a new empirical correlation for stationary crossflow vortices [12].
The original Langtry-Menter model was implemented in our in-house CFD code, BRU3D [13, 14, 15]. In this original effort, transition caused by stationary crossflow vortices was not considered. In this paper, we consider an empirical correlation for crossflow transition published in Ref. [12]. This empirical correlation is implemented in the BRU3D code. We also present a numerical study on the freestream turbulence variables and a study on the numerical convergence considering a prolate spheroid test case.

2. Methods

In the present work, an in-house developed CFD code, BRU3D [13, 14, 15], is used to simulate the flowfields of interest. The BRU3D code has been continuously improved by the research group over the years, and by now, the code can solve the Euler compressible equations and/or the Reynolds-averaged Navier-Stokes equations. Results that demonstrated the validation of the code can be found in Refs. [13, 14]. Moreover, turbulence closure can be achieved with many different turbulence models, for example, the Shear Stress Transport (SST) model [16]. More recently, the laminar-turbulent transition Langtry-Menter model [11] has also been implemented. The equations are solved in a standard, cell-centered, finite volume method for general unstructured grids. The code can be executed using parallel MPI calls.

2.1 The Shear Stress Transport Turbulence Model

In our implementation, the Langtry-Menter $\gamma - Re_\theta$ transition model [11] is coupled to the SST turbulence model [16]. The SST model is based on the Boussinesq hypothesis, in which the eddy viscosity, μ_t, is used as a means to represent the Reynolds stress tensor terms. The SST model uses a blending function, F1, to combine the advantages of the k-ε and the k-ω models. The blending function activates the k-ω model in the near wall region and the k-ε model for the rest of the flow. The SST model is composed of two equations. The first equation is for the turbulent kinetic energy, k, given by

$$\frac{\partial(\rho k)}{\partial t} + \frac{\partial(\rho u_j k)}{\partial x_j} = P_k - D_k + \frac{\partial}{\partial x_j}\left[\left(\mu + \frac{\mu_t}{\sigma_k}\right)\frac{\partial k}{\partial x_j}\right], \tag{1}$$

where ρ is the density, u_j represents the velocity vector components, P_k is the production term and D_k is the destruction term, μ is the molecular dynamic viscosity, μ_t is the eddy viscosity, and $\sigma_k = 0.85$. The second equation is for the turbulence frequency, ω, given by

$$\frac{\partial(\rho\omega)}{\partial t} + \frac{\partial(\rho u_j \omega)}{\partial x_j} = \frac{\gamma}{\nu_t}P_\omega - \beta\rho\omega^2 + \frac{\partial}{\partial x_j}\left[\left(\mu + \frac{\mu_t}{\sigma_k}\right)\frac{\partial\omega}{\partial x_j}\right] + (1-F_1)2\rho\sigma_{\omega 2}\frac{1}{\omega}\frac{\partial k}{\partial x_j}\frac{\partial\omega}{\partial x_j}, \tag{2}$$

where P_ω is the production term, $\beta = 0.09$, $\gamma = \frac{\beta_1}{\beta*} - \frac{\sigma_{\omega 1}\kappa^2}{\sqrt{\beta*}}$ with $\beta_1 = 0.075$, $\sigma_{\omega 1} = 0.5$ and $\kappa = 0.41$, and $\sigma_{\omega 2} = 0.856$.
The production term for the kinetic energy equations, P_k, is

$$P_k = \min\left(\mu_t S^2, 10 D_k\right), \tag{3}$$

where S is the strain rate magnitude, given by

$$S = \sqrt{2 S_{ij} S_{ij}}. \tag{4}$$

The destruction term for the kinetic energy equation, D_k, is

$$D_k = \beta^* \rho \omega k. \tag{5}$$

The blending function, F_1, is

$$F_1 = \tanh\left(\min\left(\max\left(\frac{\sqrt{k}}{\beta * \omega y}; \frac{500\nu}{y^2\omega}\right); \frac{4\rho\sigma_{\omega 2}k}{CD_{k\omega}y^2}\right)\right)^4, \tag{6}$$

where y is the distance from the field point to the nearest wall, and

$$CD_{k\omega} = \max\left(2\rho\sigma_{\omega 2}\frac{1}{\omega}\frac{\partial k}{\partial x_j}\frac{\partial \omega}{\partial x_j}; 1\times 10^{-10}\right). \tag{7}$$

The turbulent viscosity is calculated as follows

$$\mu_t = \min\left(\frac{\rho k}{\omega}; \frac{a_1 \rho k}{SF_2}\right), \tag{8}$$

where $a_1 = 0.31$. The F_2 term is a blending function given by

$$F_2 = \tanh\left\{\max\left(2\frac{\sqrt{k}}{\beta * \omega y}; \frac{500\mu_t}{\rho y^2 \omega}\right)\right\}^2. \tag{9}$$

Further information on the SST model can be found in Ref. [16].

2.2 The Langtry-Menter Transition Model

2.2.1 Standard Transition Model Formulation

The Langtry-Menter transition model is composed by two transport equations, which are combined with those from the original SST model. The model is based only on local variables and is compatible with modern CFD codes. In the Langtry-Menter model, the strain rate Reynolds number, which is a local variable, maps the transition momentum-thickness Reynolds number, which is nonlocal and plays an important role in transition prediction.

The first transport equation of the Langtry-Menter model is for the intermittency, γ, which is used to trigger the SST source terms. The intermittency is set to be equal to one in the regions of a fully-turbulent flow and zero in a laminar boundary layer. Also, the intermittency is set be equal to one in the freestream and it is used in the method mainly for extending the applicability of the model and the robustness of the current method. The transport equation for the intermittency has the goal of constructing the transitional flow region in a smooth manner, providing numerical stability. The γ equation is given by

$$\frac{\partial(\rho\gamma)}{\partial t} + \frac{\partial(\rho u_j \gamma)}{\partial x_j} = P_\gamma - E_\gamma + \frac{\partial}{\partial x_j}\left[\left(\mu + \frac{\mu_t}{\sigma_f}\right)\frac{\partial \gamma}{\partial x_j}\right], \tag{10}$$

where P_γ is the intermittency source term, E_γ is the destruction-relaminarization source term, and $\sigma_f = 1.0$. The intermittency represents the probability of a fluid cell to be turbulent. The second transport equation represents the transition momentum thickness Reynolds number, $\tilde{Re}_{\theta_t}$, which is written for the transition onset, and is given by

$$\frac{\partial\left(\rho\tilde{Re}_{\theta_t}\right)}{\partial t} + \frac{\partial\left(\rho u_j \tilde{Re}_{\theta_t}\right)}{\partial x_j} = P_{\theta_t} + \frac{\partial}{\partial x_j}\left[\sigma_{\theta_t}\left(\mu + \mu_t\right)\frac{\partial \tilde{Re}_{\theta_t}}{\partial x_j}\right], \tag{11}$$

where P_{θ_t} is the source term and $\sigma_{\theta_t} = 2.0$ controls the diffusion coefficient. The Reynolds number based on the momentum-thickness represents a sensor responsible for triggering the transition process, because $\tilde{Re}_{\theta_t}$ indicates the point where the transition begins. The Langtry-Menter model couples the intermittency function with the SST model to activate the turbulent kinetic energy,

$$\frac{\partial(\rho k)}{\partial t} + \frac{\partial(\rho u_j k)}{\partial x_j} = \tilde{P}_k - \tilde{D}_k + \frac{\partial}{\partial x_j}\left[\left(\mu + \sigma_k \mu_t\right)\frac{\partial k}{\partial x_j}\right], \tag{12}$$

$$\tilde{P}_k = \gamma_{eff} P_k, \tag{13}$$

$$\tilde{D}_k = \min\left(\max\left(\gamma_{eff}, 0.1\right), 1.0\right) D_k \ , \tag{14}$$

where $\tilde{P}_k$ and $\tilde{D}_k$ are the original production and destruction terms of the SST model, and $\gamma_{eff} P_k$ includes the separation effects in the formulation.
The original Langtry-Menter transition model is able to predict transition triggered by the amplification of Tollmien-Schlichting waves and bypass transition. Further information and the empirical correlations can be found in the literature [11].

2.2.2 Empirical Correlation Based on the Surface Roughness

In order to predict transition due to crossflow effects, the Langtry-Menter model was extended [12] with a new empirical correlation for stationary crossflow transition. The empirical correlation for crossflow effects is based on the streamwise vorticity ($\Omega_{\text{Streamwise}}$) as an indicator of the local crossflow strength in the boundary layer, defined as follows

$$\vec{U} = \left(\frac{u}{\sqrt{u^2+v^2+w^2}}, \frac{v}{\sqrt{u^2+v^2+w^2}}, \frac{w}{\sqrt{u^2+v^2+w^2}} \right) \ , \tag{15}$$

$$\vec{\Omega} = \left(\frac{\partial w}{\partial y} - \frac{\partial v}{\partial z}, \frac{\partial u}{\partial z} - \frac{\partial w}{\partial x}, \frac{\partial v}{\partial x} - \frac{\partial u}{\partial y} \right) \ , \tag{16}$$

$$\Omega_{Streamwise} = |\vec{U} \cdot \vec{\Omega}|. \tag{17}$$

In order to non-dimensionalize $\Omega_{Streamwise}$ into a measure of the crossflow strength, and to build an empirical correlation based on $H_{crossflow}$, the non-dimensional parameter $H_{crossflow}$ is defined as

$$H_{Crossflow} = \frac{y \Omega_{Streamwise}}{U}, \tag{18}$$

as the crossflow strength indicator, where y is the distance to the nearest wall and U is the magnitude of the nondimensional velocity vector defined in Eq. 15. The empirical correlation for crossflow effects accounts for the surface roughness on the transition momentum thickness Reynolds number,

$$Re_{SCF} = \frac{\theta_t \rho \left(\frac{U}{0.82}\right)}{\mu} = -35.088 \ln\left(\frac{h}{\theta_t}\right) + 319.51 + f(+\Delta H_{crossflow}) - f(-\Delta H_{crossflow}) \ , \tag{19}$$

where $f(+\Delta H_{crossflow})$ and $f(-\Delta H_{crossflow})$ are a shift up or down depending on the local crossflow strength, θ_t is the momentum thickness, U is the velocity magnitude, ρ is the density, and h is the rms surface roughness height. The crossflow effect is implemented as a stationary crossflow sink term D_{SCF} in the Re_{θ_t} transport equation as

$$\frac{\partial(\rho \tilde{Re}_{\theta_t})}{\partial t} + \frac{\partial(\rho u_j \tilde{Re}_{\theta_t})}{\partial x_j} = P_{\theta_t} + D_{SCF} + \frac{\partial\left[\sigma_{\theta_t}(\mu + \mu_t)\frac{\partial \tilde{Re}_{\theta_t}}{\partial x_j}\right]}{\partial x_j}, \tag{20}$$

where

$$D_{SCF} = c_{\theta_t} \frac{\rho}{t} c_{Crossflow} \min\left(Re_{SCF} - \tilde{Re}_{\theta_t}, 0.0\right)(F_{\theta_t 2}) \ , \tag{21}$$

$$F_{\theta_t 2} = \min\left(F_{wake} e^{-(y/\delta)^4}, 1.0\right) \ , \tag{22}$$

where $c_{crossflow} = 0.6$, and $F_{\theta_t 2}$ confines the crossflow sink term D_{SCF} so that it is only activated inside the boundary layer, and F_{wake} is given by

$$F_{wake} = exp\left[-\left(\frac{Re_w}{1 \times 10^5} \right)^2 \right] \ , \tag{23}$$

where

$$Re_w = \frac{\rho \Omega y^2}{\mu} \ , \tag{24}$$

and Ω is the vorticity magnitude. Further information on the details of the above empirical correlation for the prediction of crossflow instabilities can be found in the literature [12].

2.3 Numerical Formulation

In the present work, we use the finite-volume method for spatial discretization [17]. The equations are discretized using a cell-centered, finite volume approach for general unstructured grids [13, 18]. The Roe approximate Riemann solver [19] is used for the calculation of the numerical fluxes associated with the inviscid terms at cell interfaces. A MUSCL reconstruction approach is implemented in order to achieve 2nd-order accuracy and appropriate limiter functions are used in the reconstruction process to obtain a monotonic stable solution over shock waves [18]. This is a very standard approach for handling typical aerospace applications which include shock waves. Discretization of the viscous flux terms use standard, volume-weighted averages of the mean cell gradients [20]. Further information on the details of the spatial discretization approach adopted in the present work can be found in Refs. [18, 20]. A point-implicit time integration scheme, based on the first-order backward Euler method, is used for the temporal discretization of the governing equations and it contributes to achieve better numerical robustness [18].

3. Results

The validation of the Langtry-Menter transition model, that was originally implemented in the BRU3D code, can be found in Ref. [20]. In previous work by the present authors, two test cases for zero-pressure gradient flat plates [21, 22], accounting for transition caused by the amplification of Tollmien-Schlichting (TS) waves (Case A) and bypass transition (Case B), were also addressed. The test cases used a 5 million Reynolds number, Mach number of 0.2, and three different meshes. For Case A, we considered a flow condition with a freestream turbulence intensity, Tu_i, lower than 1%, which characterizes transition caused by TS waves. For Case B, we considered Tu_i larger than 1%, which represents bypass transition, and this is the main difference between both test cases. Moreover, the initial studies also included the simulation of the flow over the NLF(1)-0416 airfoil [23] for transition caused by TS waves. The test case used a 4 million Reynolds number, angle of attack of 0 deg, Mach number of 0.2, and Tu_i of 0.15% and 0.3%. All test cases included results for the skin friction coefficient (c_f), thus it is possible to observe where the transition to turbulence starts. Further information can be found in Ref. [24].

In the present paper, our first results for the Langtry-Menter model are based on a prolate spheroid test case for which transition is triggered by the amplification of TS waves. The experimental study for the 6:1 inclined prolate spheroid test case was performed at the low speed wind tunnel DLR in Göttingen [25]. For the experimental cases, the freestream turbulence intensity in the wind tunnel was in the range of $Tu_{\text{inf}} \approx 0.1\%$ considering different test conditions for transition only due to Tollmien-Schlichting waves, transition caused by Tollmien-Schlichting waves and crossflow instabilities, and transition caused by crossflow instabilities only. A few operational test conditions for computations were considered for the transition cases mentioned before and published in [26]. For the case with transition only due the amplification of Tollmien-Schlichting waves, the authors considered for the computational simulations a flow condition with 1.5 millions Reynolds number, a 10-degree angle of attack, a 0.03 Mach number, a freestream turbulence intensity at the farfield of 1.0%, and an eddy viscosity to molecular viscosity ratio, μ_t/μ_{ref}, of 5.0.

The c_f values in the turbulent flow region are smaller for the computational results in Ref. [26] than in the experiment [25], but if the area of increasing c_f indicates the transition region, the experimental and computational results are in good agreement [26]. Our numerical results for transition due to TS waves are confronted with the results obtained in Ref. [25] for the c_f contours through the white line in our own plots, indicating the transition front extracted from the reference results. For our numerical simulation, the reference freestream parameters were chosen in order to verify our numerical solution behavior and are shown in Table 1. Figure 1 depicts our numerical results obtained with the BRU3D code, where the region where the skin friction contours shift from blue to yellow represents

the transition front location. Confronting our numerical results with the white line from the reference mentioned before, we observe good agreement between the results.

Table 1 – Reference freestream values for test case with transition due to amplification of TS waves.

alpha	Re	Mach	Tu$_i$%	μ_t/μ_{ref}
10	1.5×10^6	0.14	0.2	100

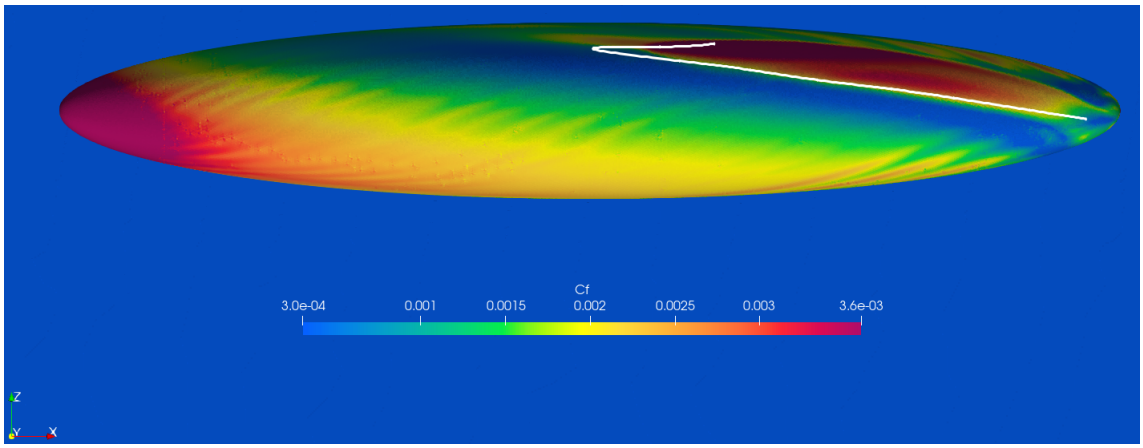

Figure 1 – Skin friction contours obtained with the BRU3D code for the case of transition due to amplification of TS waves.

Figure 2 shows the residual convergence for the L-infinity norm for the four turbulent variables, k, ω, γ, and Re_{θ_t} for the results shown in Fig. 1. As mentioned before, this test case consists of transition caused by the amplification of Tollmien-Schlichting waves using the setup of the freestream turbulence variables shown in Table 1. It is possible to see that the equation for γ has the best convergence rate. Both equations of the SST turbulence model hold similar convergence rates. The second equation of the Langtry-Menter transition model, corresponding to the Re_{θ_t} variable, has a lower convergence rate. We observe that, after 6000 iterations, the residuals stall and high-frequency noise is observed. This behavior is typical of transitional flow simulations and may be caused by the intermittency field oscillations in the near wall cells. Figures 3 and 4 display the behavior of the lift coefficient, C_L, and the drag coefficient, C_D, respectively, over the iteration cycles. It is possible to observe through the force coefficients behavior where the values of C_L and C_D stop changing and the numerical solution converges. The maximum number of 30,000 iterations are sufficient for a converged numerical simulation. The lift and drag coefficients histories reveal that, even with the noise observed in the flow residuals, the force coefficients are converged.

We also include results corresponding to the newly implemented empirical correlation for stationary crossflow transition found in Ref. [12] for the prolate spheroid, which is a well known test case for stationary crossflow transition. The investigations include the analyses of the impact of the freestream variables on the numerical results, as well as the effect of the empirical correlations that aim to reproduce the stationary crosflow transition on the residual convergence. The result is confronted with the numerical result for stationary crossflow transition found in Ref. [12], which is represented here by the yellow line superimposed to our numerical results. In Ref. [12], the authors consider a Reynolds number of 6.5 million, an angle of attack of 15 degrees, a freestream turbulence intensity of 0.1%, and a surface roughness of 3.3 μm. The results for the skin friction coefficient are obtained with the unstructured BCFD code and with the OVERFLOW code. According to Ref. [12], OVERFLOW results present an early transition for the crossflow modification, but good agreement with the experimental data is observed.

The flow conditions for the test cases are presented in Table 2. Table 3 presents the freestream turbulence, numerical parameters, and mesh information for the present test cases with transition due to stationary crossflow vortices, where T_u is the freestream turbulent intensity, μ_t/μ_{ref} is the eddy

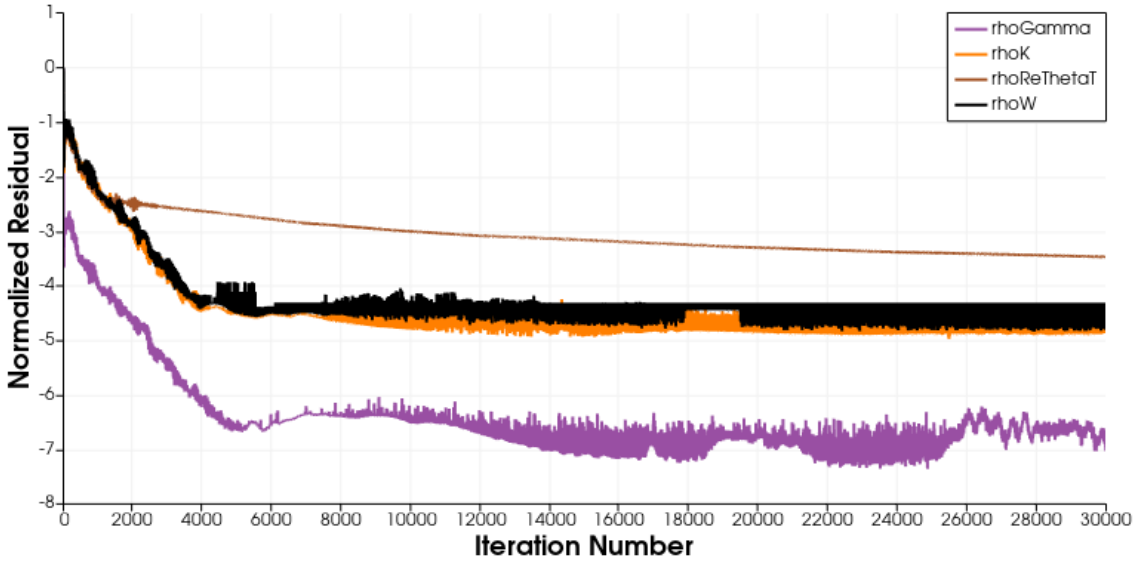

Figure 2 – Residual convergence for the turbulent variables for the test case of transition due to amplification of TS waves.

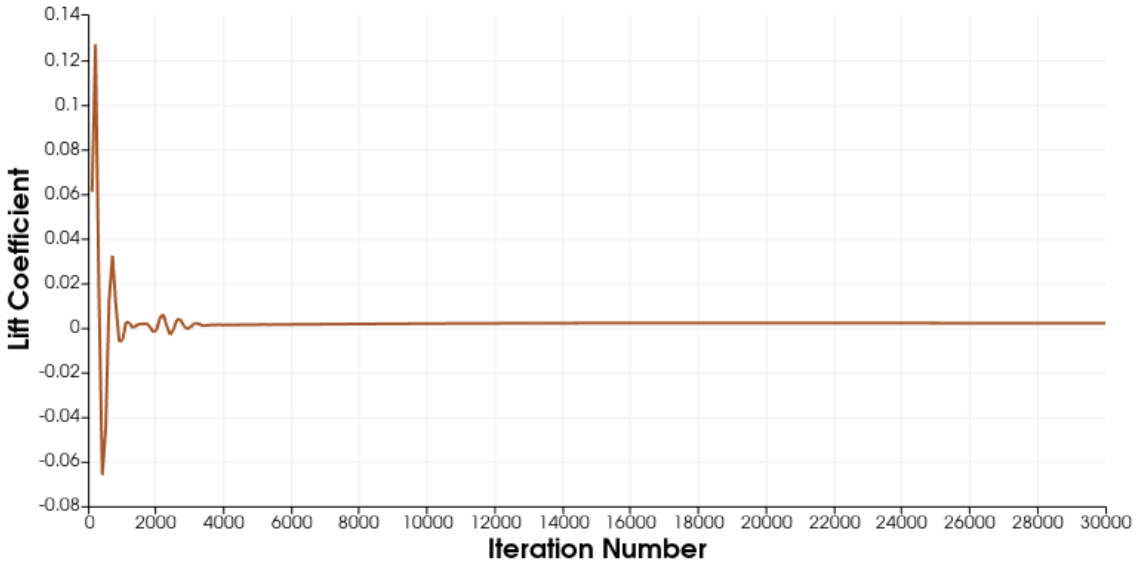

Figure 3 – Lift coefficient, C_L, obtained for the test case of transition due to the amplification of TS waves.

viscosity to molecular viscosity ratio, and α_{ROE} represents the value for the entropy fix parameter for the Roe scheme [18].

Table 2 – Flow conditions for the test case with crossflow transition.

alpha	Re	Mach	h (μm)
15	6.5×10^6	0.14	3.3

Case 1 is represented in Fig. 5 with the skin friction coefficient contours. The region on the surface where the contours shift from blue to red represents the transition front location. If the region with the increasing values of c_f represents the transition location, our numerical results display a delayed transition. Also, our transition front shows an unexpected zig zag-like behavior.
Our numerical solution for the c_f contours for Case 2 is represented in Fig. 6. The main difference between Case 1 and Case 2 is the value of the α_{ROE}, as indicated in Table 3. We observe similar

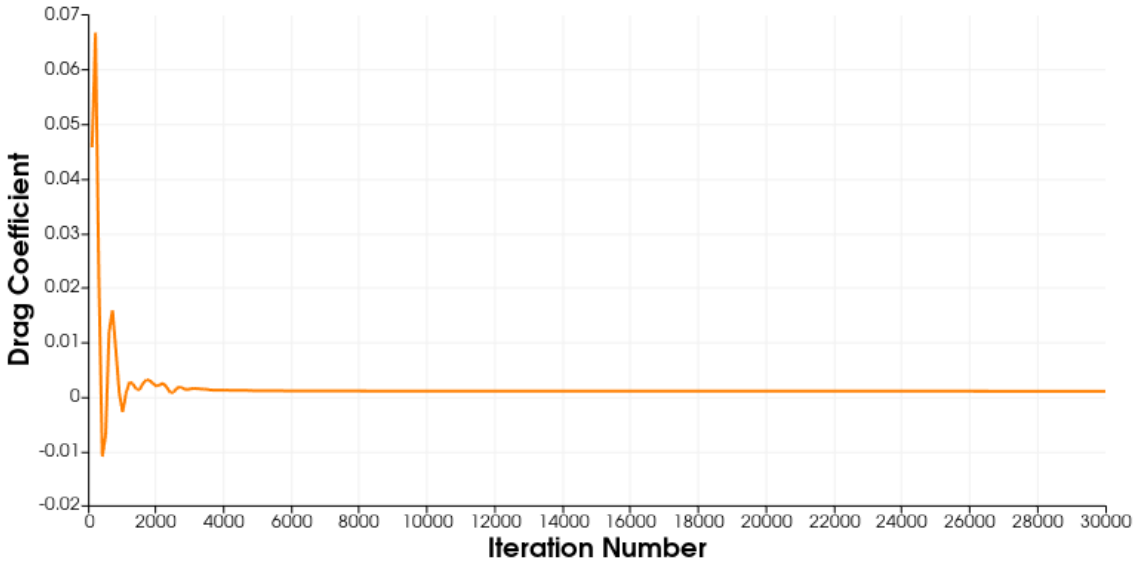

Figure 4 – Drag coefficient, C_D, obtained for the test case of transition due to the amplification of TS waves.

Table 3 – Additional simulation data for the stationary crossflow test case, including freestream turbulence properties.

Case	T_u	μ_t/μ_{ref}	α_{ROE}	Mesh (Total nodes)
Case 1	0.1%	10	0.035	2,715,698
Case 2	0.1%	10	0.05	2,715,698
Case 3	0.1%	100	0.01	2,715,698

values for the c_f contours, as well as the shape of the transition front contour. However, the region of increasing values of c_f for the transition location is not delayed as in Case 1, but still less regular than expected in the yellow line, representing the results from Ref. [12].
Case 3 is represented in Fig. 7 with the skin friction coefficient contours. For Case 3, the values of μ_t/μ_{ref} and α_{ROE} are different from Case 1 and Case 2, as previously indicated. As for cases previously studied, we observe a delayed transition region indicated by the c_f contours. However, the transition front contour is more regular as expected for this case than for the other two cases studied. In general, we observe some discrepancy between our numerical results and the ones obtained in Ref. [12]. More tests are currently being performed in order to fully understand the numerical results with the BRU3D code. It must be emphasized that numerical characteristics of a particular code might cause variations on the freestream turbulence properties that must be specified at farfield boundaries, as already discussed in previous work [8]. Therefore, the discrepancies observed in the present work might have their origins on different numerics as well as on a calibration of farfield turbulent properties.
Our final results aim to investigate the new correlations impact on the convergence behavior. Figure 8 shows the residual convergence for the L-infinity norm for the four turbulence variables, k, ω, γ, and Re_{θ_t} for the results shown in Fig. 5 for Case 1. For a matter of brevity, the numerical convergence for Case 2 and Case 3 are not presented here since their overall behaviors are similar to those depicted in Fig. 8. For these test cases, the transition is dominated by crossflow vortices. We can see that the ω variable holds similar convergence rate comparing to k and γ equations. Despite of having a slightly better residual convergence, the three turbulence variables display similar convergence rates. The level of residual convergence achieved for Re_{θ_t} is still lower when compared to the other turbulence variables, as seen before. After 10,000 iterations, we observe that the residuals values stop decreasing and high-frequency noisy is observed, which is typical of transitional flow simulations. Figures 9 and 10 show the C_L and C_D curves, respectively, for Case 1. We observe that after 4,000

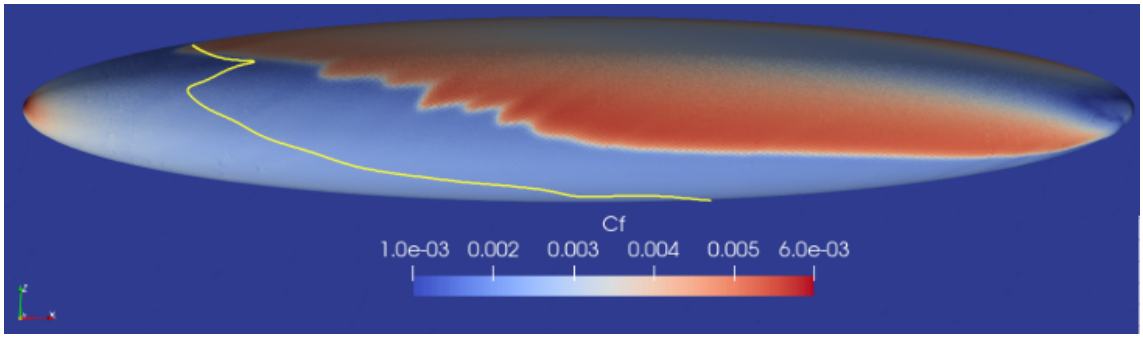

Figure 5 – Skin friction coefficient contours for Case 1.

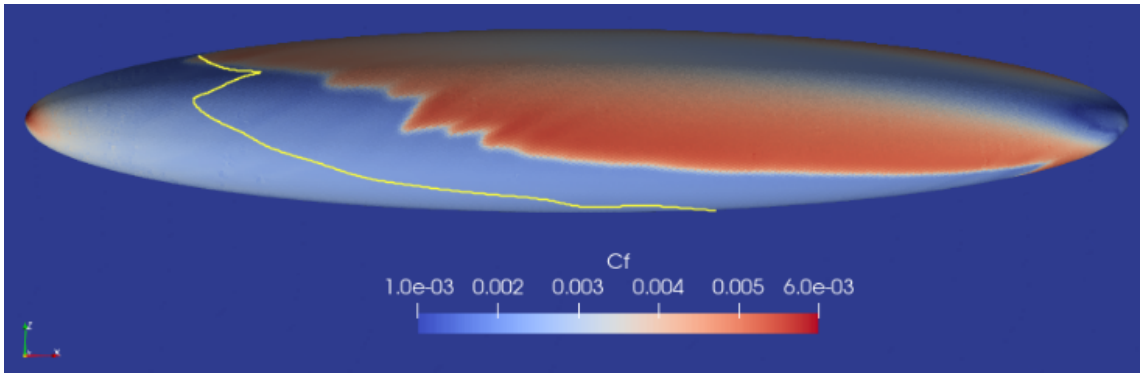

Figure 6 – Skin friction coefficient contours for Case 2.

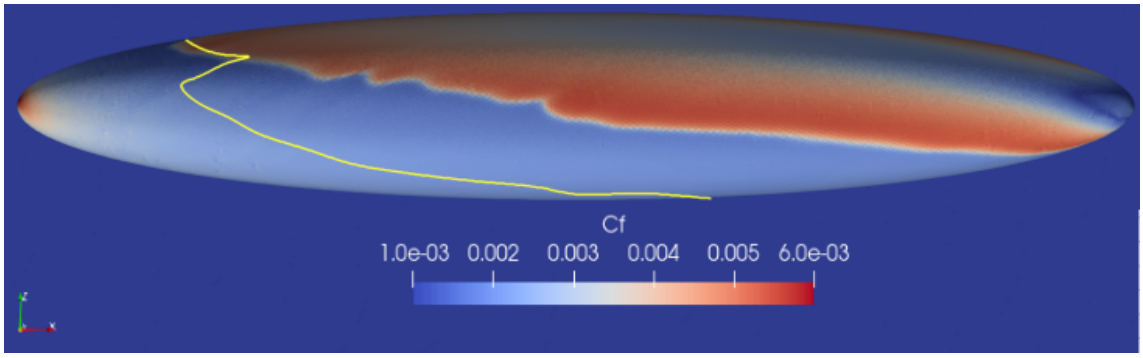

Figure 7 – Skin friction coefficient contours for Case 3.

iterations the values of the force coefficients are converged. The maximum iteration number of 30,000 is enough to obtain a converged numerical solution. Comparing the convergence histories shown in Figs. 2 and 8, it is possible to see that, after adding the new empirical correlations to the model, the level of residual reduction that one is able to achieve is lower in the present case than what was achieved with the standard Langtry-Menter transition model. This behavior is caused by the nonlinearities present in the stationary crossflow empirical correlations which add stiffness to the numerical problem.

4. Conclusions

The present study considers the use of different versions of the Langtry-Menter transition model, which is implemented in an in-house code, BRU3D. In a previous work, the code was validated for a flat plate test case considering transition caused by Tollmien-Schlichting waves and bypass transition, and for the NLF(1)-0416 airfoil test case for transition caused by the amplification of Tollmien-Schlichting waves. In the present work, we focus on the prolate spheroid test case, for which we first perform a comparison with experimental values for transition caused by the amplification of Tollmien-Schlichting waves in order to validate the transition model. We obtained numerical results in good

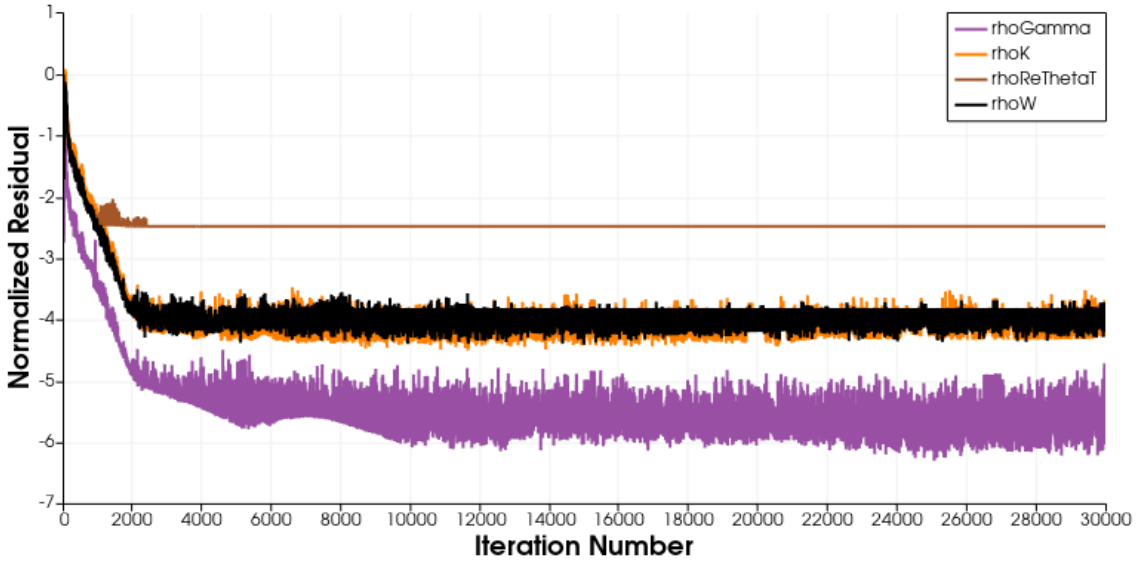

Figure 8 – Residual convergence for crossflow-triggered transition Case 1.

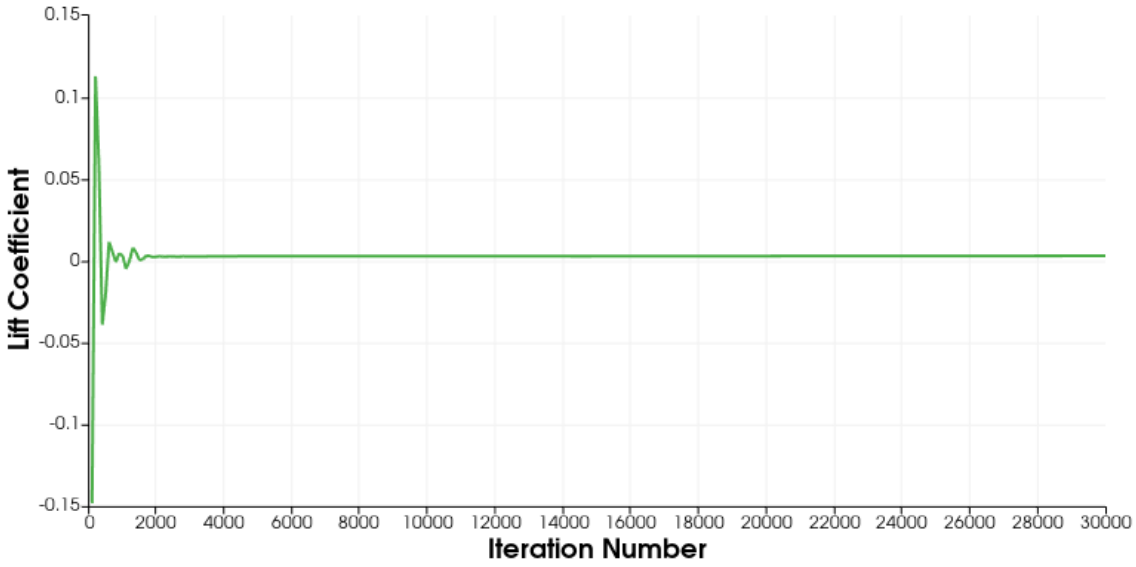

Figure 9 – Lift coefficient, C_L, obtained for the test case of transition due to stationary crossflow instabilities for Case 1.

agreement with the experimental data available in the literature.

The empirical correlation for crossflow transition was implemented in the BRU3D code. We started our numerical tests for transition caused by crossflow analyzing the skin friction coefficient, c_f. We observe that our numerical results present some mismatches when compared to the data available in the literature. On the other hand, it is worth mentioning that the addition of crossflow effects lead to a transition front whose overall topology is similar to the results obtained by other research groups. We also point out that the nonlinearities included in the stationary crossflow empirical correlations add numerical stiffness to the problem, resulting in overall higher levels of residuals for all turbulence variables at the final converged solution. In other words, the ability to reduce the residuals for the turbulence variables is decreased by the additional stiffness. This observation is in agreement with results in the literature and highlights the relevance of devising strategies to converge transitional RANS models.

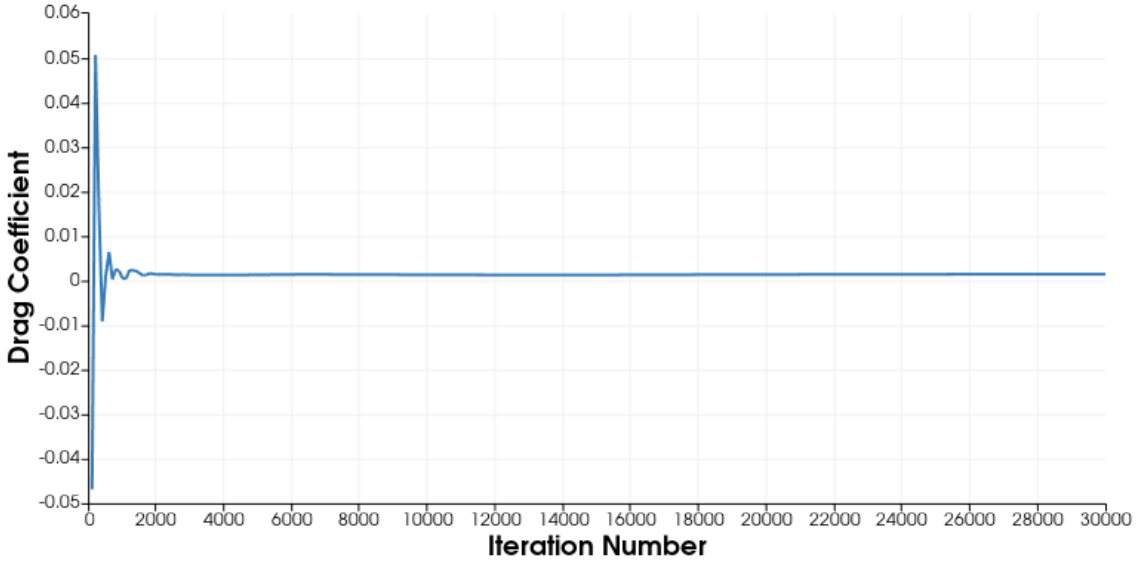

Figure 10 – Drag coefficient, C_D, obtained for the test case of transition due to stationary crossflow instabilities for Case 1.

5. Acknowledgments

The authors gratefully acknowledge the support provided by Fundação de Amparo à Pesquisa do Estado de São Paulo, FAPESP, through a doctoral scholarship for the first author under Grant No. 2021/00031-0. The simulations in the present work would not be possible without the computational resources from the Center for Mathematical Sciences Applied to Industry (CeMEAI), funded by FAPESP under the Research Grant No. 2013/07375-0. Additional support to the third author under the FAPESP Research Grant No. 2013/07375-0 is also gratefully acknowledged. Further support for the present research was provided by Conselho Nacional de Desenvolvimento Científico e Tecnológico, CNPq, under the Research Grant No. 309985/2013-7.

6. Contact Author Email Address

Aline R. Santos Righi: alinerighi29@gmail.com Tel. +55 12 3947-5813
Gustavo Luiz Olichevis Halila: gustavo.halila@embraer.com.br
João Luiz F. Azevedo: joaoluiz.azevedo@gmail.com Tel. +55 12 3947-6488

7. Copyright Statement

References

[1] Versteeg, K. H. and Malalasekera, W., *An Introduction to Computational Fluid Dynamics*, Pearson Education Limited, 2nd ed., 2007.

[2] Klebanoff, P. S., Tidstrom, K. D., and Sargent, L. M., "The Three-Dimensional Nature of Boundary Layer Instability," *Journal of Fluid Mechanics*, Vol. 12, 1962, pp. 1–24.

[3] Ghasemi, E., McEligot, D., Nolan, K., Crepeau, Siahpush, A., Budwig, R., and Tokuhiro, A., "Effects of Adverse and Favorable Pressure Gradients on Entropy Generation in a Transitional Boundary Layer Region Under the Influence of Freestream Turbulence," *International Journal of Heat and Mass Transfer*, Vol. 77, 2014, pp. 475–488.

[4] Saric, W. S. and Dagenhart, J. R., "Crossflow Stability and Transition Experiments in Swept-Wing Flow," NASA TP-1999-209344, NASA, July 1999.

[5] Poll, D. I. A., "Some Aspects of the Flow Near a Swept Attachment Line with Particular Reference to Boundary Layer Transition," College of Aeronautics TR 7805, College of Aeronautics, Cranfield, England, UK, August 1978.

[6] Halila, G. L. O., Antunes, A. P., Silva, R. G., and Azevedo, J. L. F., "Effects of Boundary Layer Transition on the Aerodynamic Analysis of High-lift Systems," *Aerospace Science and Technology*, Vol. 90, July 2019, pp. 233–245.

[7] Halila, G. L. O., Bigarella, E. D. V., and Azevedo, J. L. F., "A Numerical Study on Transitional Flows Using a Correlation-Based Transition Model," *Journal of Aircraft*, Vol. 53, No. 4, July–August 2016, pp. 922–941.

[8] Halila, G. L. O., Bigarella, E. D. V., Antunes, A. P., and Azevedo, J. L. F., "An Efficient Setup for Freestream Turbulence on Transition Prediction over Aerospace Configurations," *Aerospace Science and Technology*, Vol. 81, October 2018, pp. 259–271.

[9] Smith, A., Company, D. A., Gamberoni, N., Sub-Committee, A. R. C. F. M., and Department, D. A. C. E. S. D. E., *Transition, Pressure Gradient and Stability Theory*, ARC-19322, Douglas Aircraft Company, El Segundo Division, 1956.

[10] van Ingen, L. J., "A Suggested Semi-Empirical Method for the Calculations of the Boundary Layer Transition Region," Dept. Aerospace Engineering VTH 74, University of Delft, Delft, The Netherlands, 1956.

[11] Langtry, R. B. and Menter, F. R., "Correlation-Based Transition Modeling for Unstructured Parallelized Computational Fluid Dynamics Codes," *AIAA Journal*, Vol. 47, No. 12, 2009, pp. 2894–2906.

[12] Langtry, R. B., Sengupta, K., Yeh, D. T., and Dorgan, A. J., "Extending the γ - Re Local Correlation based Transition Model for Crossflow Effects," *Proceedings of the 2015 AIAA Fluid Dynamics Conference, AIAA Aviation Forum,* AIAA Paper No. 2015-2474, Dallas, TX, June 2015.

[13] Bigarella, E. D. V. and Azevedo, J. L. F., "Advanced Eddy-Viscosity and Reynolds-Stress Turbulence Model Simulations of Aerospace Applications," *AIAA Journal*, Vol. 45, No. 10, Oct. 2007, pp. 2369–2390.

[14] Bigarella, E. D. V., *Advanced Turbulence Modelling for Complex Aerospace Applications*, Ph.D. thesis, Instituto Tecnológico de Aeronáutica, São José dos Campos, Brazil, 2007.

[15] Carvalho, L. M. M. O., *Numerical Study of Transitional Flows Over Aerospace Configurations*, Master's thesis, Instituto Tecnológico de Aeronáutica, São José dos Campos, Brasil, 2018.

[16] Menter, F. R., "Two-Equation Eddy Viscosity Turbulence Models for Engineering Applications," *AIAA Journal*, Vol. 32, No. 8, 1994, pp. 1598–1605.

[17] Hirsh, C., *Numerical Computation of Internal and External Flows*, Wiley, 1990.

[18] Bigarella, E. D. V. and Azevedo, J. L. F., "A Unified Implicit CFD Approach for Turbulent-Flow Aerospace-Configurations Simulations," *Proceedings of the 47th AIAA Aerospace Sciences Meeting Including the New Horizons Forum and Aerospace Exposition*, Orlando, FL, Jan. 2009.

[19] Roe, P. L., "Approximatte Riemann Solvers, Parameter Vector, and Difference Schemes," *Journal of Computational Physics*, Vol. 43, No. 2, 1981, pp. 357–372.

[20] Carvalho, L. M. M. O., da Silva, R. G., and Azevedo, J. L. F., "Numerical Study of Transitional Flows Over Aerospace Configurations," AIAA Paper No. 2018-4209*, Proceedings of the 2018 AIAA Applied Aerodynamics Conference, AIAA Aviation Forum*, June 2018.

[21] Rumsey, C. L. and Lee-Rausch, E. M., "NASA Trapezoidal Wing Computations Including Transition and Advanced Turbulence Modeling," *Journal of Aircraft*, Vol. 52, 2015, pp. 496–509.

[22] Coder, J. G., "Standard Test Cases for Transition Model Verification and Validation in Computational Fluid Dynamics," AIAA Paper No. 2018-0029*, Proceedings of the 2018 AIAA Aerospace Sciences Meeting, AIAA SciTech Forum*, Kissimmee, FL, Jan. 2018.

[23] Somers, D. M., "Design and Experimental Results for a Natural-Laminar-Flow Airfoil for General Aviation Applications," Tech. Rep. NASA TP-1681, National Aeronautics and Space Administration – NASA, 1981.

[24] Righi, A. R. S., Carvalho, L. M. M. O., Halila, G. L. O., and Azevedo, J. L. F., "A Numerical Study on the Effects of Mesh Refinament, Artificial Dissipation, and Freestream Turbulence on Laminar-Turbulent Transition Predictions," *Proceedings of the 26th International Congress of Mechanical Engineering, COBEM-2021*, Virtual Congress, Brazil, November 2021.

[25] Kreplin, H. P., Vollmers, H., and Meier, H. U., "Wall Shear Stress Measurements on an Inclined Prolate Spheroid in the DFVLR 3m x 3m Low Speed Wind Tunnel, Göttingen," Tech. Rep. IB-22-84-A-33, DFVLR-AVA, 1985.

[26] Grabe, C. and Krumbein, A., "Transition Transport Modeling for Three-Dimensional Aerodynamic Configurations," *Journal of Aircraft*, Vol. 50, No. 5, 2013, pp. 1535–1539.